Journal of Oncology Research and Therapy
Narayanasamy B, et al. Oncol Res Ther 10: 10301.
www.doi.org/10.29011/2574-710X.10301
www.gavinpublishers.com

OPEN ACCESS

GAVIN PUBLISHERS

Research Article

DZ-1–Artesunate Induces Apoptosis Via a Bid-, Bax-, and Bak-Independent Caspase-3 Activation Pathway

Badrinath Narayanasamy[1], Sarah Helmueller[1], Yi Zhang[1], Alexandra Gangi[2], Heuiran Lee[3,4], Cheryn Song[5], Ha-Na Woo[6], and Yong J. Lee[1*]

[1]Department of Biomedical Sciences, Cedars-Sinai Medical Center, Los Angeles, CA 90048, USA.

[2]Department of Surgery, Cedars-Sinai Medical Center, Los Angeles, CA 90048, USA

[3]Bio-Medical Institute of Technology, University of Ulsan, College of Medicine, Seoul, Korea.

[4]Department of Microbiology, Asan Medical Center, University of Ulsan, College of Medicine, Seoul, Korea.

[5]Department of Urology, Asan Medical Center, University of Ulsan, College of Medicine, Seoul, Korea.

[6]Department of Biochemistry and Molecular Biology, University of Ulsan, College of Medicine, Seoul, Korea.

***Corresponding author:** Yong J. Lee, Department of Biomedical Sciences, Cedars-Sinai Medical Center, Los Angeles, CA 90048, USA.

Citation: Narayanasamy B, Helmueller S, Zhang Y, Gangi A, Lee H, et al. (2025) DZ-1–Artesunate Induces Apoptosis Via a Bid-, Bax-, and Bak-Independent Caspase-3 Activation Pathway. J Oncol Res Ther 10: 10301. DOI: 10.29011/2574-710X.10301.

Received Date: 19 August, 2025; **Accepted:** 26 August, 2025; **Published Date:** 29 August, 2025.

Abstract

Artesunate (ART), a well-established antimalarial agent, has demonstrated promising anticancer activity in both in vitro and in vivo studies. Despite its potential, clinical application of ART in oncology is limited by modest efficacy and dose-limiting toxicity, likely due to nonspecific accumulation in normal tissues. Targeted delivery strategies are therefore essential to enhance therapeutic selectivity and reduce off-target effects. To this end, ART has been conjugated with targeting molecules such as aptamers, dyes, and polymers. DZ-1, a heptamethine cyanine dye, selectively accumulates in cancer cells through overexpression of organic anion transporting polypeptides (OATPs), offering a promising vehicle for tumor-specific delivery. In this study, we evaluated the anticancer efficacy and underlying mechanisms of a novel conjugate of DZ-1 and ART (DZ-1-ART) in three human cancer cell lines: colon cancer (HCT116), pancreatic cancer (BxPC-3), and breast cancer (MCF-7). DZ-1-ART induced time-dependent cytotoxicity across all tested cancer cell lines. Mechanistically, DZ-1-ART localized to both mitochondria and lysosomes, but functional studies indicated that lysosomes were not essential for its pro- apoptotic activity. Instead, DZ-1-ART triggered mitochondria-mediated apoptosis via a Bid-, Bax-, and Bak-independent pathway, leading to caspase-3 activation and cell death. Our findings demonstrate that DZ-1-ART undergoes intracellular trafficking through lysosomes and mitochondria, but induces apoptosis primarily through a mitochondrial, Bid-Bax/Bak- independent, caspase-3-dependent pathway. These results support the development of DZ-1- ART as a tumor-targeted anticancer agent with potential applications in theranostics.

Keywords: Heptamethine Carbocyanine DZ-1; Artesunate; Caspase-3; Mitochondria; Apoptosis;

Abbreviations Used in This Paper:

ART-Artesunate;

Bak-Bcl-2 homologous antagonist killer;

Bax-Bcl-2–associated X protein;

Bcl-2-B-cell lymphoma 2;

Bcl-xL-B-cell lymphoma-extra-large;

BiP-binding immunoglobulin protein;

CatB-cathepsin B; CatD, cathepsin D;

CHOP-C/EBP homologous protein;

CML-chronic myeloid leukemia;

CREB-cAMP response element-binding protein;

CRT-calreticulin; DCs, dendritic cells;

DLBCL-diffuse large B cell lymphoma, DR5, death receptor 5;

ER-endoplasmic reticulum;

ERK-extracellular signal-regulated kinase;

HCC-hepatocellular carcinoma;

HIF1α-hypoxia-inducible factor 1-α;

HMCDs-heptamethine cyanine dyes;

HRP-horseradish peroxidase;

IRE1α-inositol-requiring enzyme 1 alpha;

MMP-mitochondrial membrane potential;

MMP-2-matrix metalloproteinase 2;

MMP-9-matrix metalloproteinase 9;

NIR-near-infrared;

OATPs-organic anion-transporting polypeptides;

PARP-1-poly [ADP- ribose] polymerase 1;

PLGA-poly-D, L-lactide-co-glycolide;

p-IRE1α-phosphorylated IRE1α, RPMI, Roswell park memorial institute;

ROS-reactive oxygen species;

STAT-3-signal transducer and activator of transcription-3, STAT5, signal transducer and activator of transcription 5; TRAIL-tumor necrosis factor-related apoptosis-inducing ligand.

Introduction

Artesunate (ART) is a derivative of artemisinin which is isolated from Artemisia annua [1]. ART is an antimalarial agent, and it is widely used for the treatment of Plasmodium falciparum infection [2]. Reactive oxygen species (ROS) generation by ART can cause damage in proteins, lipids, and nucleic acids in parasites, which can lead to the parasites' death [3]. Due to its ROS generation capacity, the anticancer properties of ART have been studied in various cancer models [4-7].

The anticancer mechanism of ART has been extensively studied in both in vitro and in vivo models [8]. ART-induced cell deaths are executed through apoptosis, autophagy and autophagy. In A375 melanoma cells, ART treatment induces inhibited expression of signal transducer and activator transcription-3 (STAT-3), matrix metalloproteinase 2 (MMP-2), matrix metalloproteinase 9 (MMP-9), myeloid cell leukemia 1 (Mcl-1) and B-cell lymphoma-extra large (Bcl-xL) which leads to apoptosis [4]. ART induces autophagy through reactive oxygen species (ROS) mediated endoplasmic reticulum (ER) stress and up-regulation of binding immunoglobulin protein (BiP), inositol-requiring enzyme 1 alpha (IRE1α), phosphorylated IRE1α (p-IRE1α), C/EBP homologous protein (CHOP), and death receptor 5 (DR5) in HCT116 and SW480 colon cancer cells [9]. In diffuse large B cell lymphoma (DLBCL) cells, ART treatment downregulates STAT-3 signaling and induces apoptosis, autophagy and ferroptosis [10]. In chronic myeloid leukemia (CML) KBM-5 xenograft model, intraperitoneal injection of ART inhibits p38, extracellular signal-regulated kinase (ERK), signal transducer and activator of transcription 5 (STAT5), cAMP response element-binding protein (CREB) activation, and tumor growth [11]. A dose-dependent tumor regression has been reported in ART treated Panc-1 xenograft tumor model [12].

However, a modest clinical efficacy and dose-limiting toxicities were reported in a phase I study of intravenous ART received cancer patients [13]. The reason for the modest clinical efficacy is perhaps due to nonspecific targeting and rapid clearance from the body. To overcome these hurdles, especially for targeting cancer cells, ART was loaded into poly-D, L-lactide-co- glycolide (PLGA), used as nanoparticles for drug delivery purpose [14, 15]. In addition, to locate and kill cancer cells, ART conjugation with dyes has been developed for theranostic purposes [16, 17].

The major purpose of theranostics is to specifically target and kill cancer cells while not affecting normal cells. Heptamethine cyanine dyes (HMCDs) are a class of fluorescent dyes, which are widely used for biomedical imaging due to their near-infrared (NIR) emission, and noninvasive nature of NIR light [18]. HMCDs such as IR-780, IR-783, MHI-148, and DZ-1 have been extensively studied for tumor targeting [19-21]. Aberrant and over expression of organic anion transporting polypeptides (OATPs) in cancer cells mediates cellular uptake of HMCDs [22, 23]. Among these dyes, DZ-1 shows high tumor selectivity, excellent stability and easy chemical nature for conjugation [24-26].

In this study, we conjugated DZ-1 to ART and investigated the cellular cytotoxic effects, uptake, mode of action, and molecular mechanisms underlying the cytotoxicity of the DZ-1-ART conjugate. The results showed mitochondria and lysosomes-mediated cellular uptake, and apoptosis involved cell deaths in DZ-1-ART treated cells. Interestingly, Bax (Bcl-2-associated X protein), Bak (Bcl-2 antagonist/killer 1) and Bid (BH3 interacting-domain death agonist)- independent DZ-1-ART-induced apoptosis, but caspase-3-dependent DZ-1-ART-induced apoptosis was observed.

Methods Cell Culture

Human colon cancer cell line HCT116, human pancreatic cancer cell line BxPC-3, and human breast cancer cell line MCF-7

were purchased from American Type Culture Collection (ATCC, Manassas, VA, USA). Bax knockout (Bax-/-), Bak knockout (Bak-/-), Bid knockout (Bid-/-) and double knockout Bax and Bak (Bax−/−Bak−/−) HCT116 cells were obtained from Dr. B. Vogelstein (Johns Hopkins University, Baltimore, MD, USA). These cell lines were maintained in Roswell Park Memorial Institute (RPMI)-1640 medium (Gibco, Grand Island, NY, USA). MCF-7/Vector and MCF-7/Caspase3 were obtained from Dr. C. J. Froelich (Northwestern University, Chicago, IL, USA). These cell lines were maintained in Dulbecco's Modified Eagle medium (DMEM) (Gibco, Grand Island, NY, USA). These media were maintained with 10% fetal bovine serum (FBS) (R&D Systems, McKinley Place NE, MN, USA) and cultured in a humidified atmosphere of 5% CO2 at 37ºC.

Chemical and Reagents

ART (Cat#A3731), and E-64 (Cat#E3132-1 MG) were purchased from Millipore Sigma (Saint Louis, MO, USA) Pepstatin A (Cat#1190/10) was purchased from Bio-Techne (Minneapolis, MN, USA). Z-VAD-FMK (Cat# S7023) and Z-DEVD-FMK (Cat# S7312) were purchased from Selleckchem (Houston, TX, USA). DZ-1 and DZ-1-ART were synthesized by Dr. Yi Zhang (Cedars-Sinai Medical Center, Los Angeles, CA, USA).

Cell Survival Assay

For cell survivals, trypan blue exclusion assay was used. To differentiate live and dead cells, after specific time of DZ-1-ART, E-64, pepstatin A, Z-VAD-FMK and Z-DEVD-FMK treatment, cells were stained with 0.4% trypan blue. LUNA™ Automated Cell Counter (L10001, Logos BioSystem, Anyang, Gyeonggi-do, South Korea) was used to count dead cells and live cells.

Immunoblotting and Antibodies

Immunoblotting was performed as previously described [27]. Primary antibodies, such as anti- PARP-1 (Rabbit mAb; Cat #9532S), anti-caspase-8 (Mouse mAb; Cat #9746S), anti-cleaved caspase-9 (Rabbit mAb; Cat #7237S), anti-caspase-3 (Mouse mAb; Cat#9668S), anti-cleaved caspase-3 (Rabbit mAb; Cat# 9664S), anti-Bak (Rabbit mAb; Cat #12105S), anti-Bax (Rabbit pAb; Cat #2772S), anti-Bid (Rabbit pAb; Cat#2002S), anti-cathepsin B (Rabbit mAb; 31718S) and anti-cathepsin D (Rabbit pAb; 69854S) were purchased from Cell Signaling Technology (Danvers, MA, USA). Anti-β-actin (Mouse mAb; Cat #A1978) was purchased from Sigma- Aldrich (Saint Louis, MO, USA). For secondary antibodies, anti-rabbit IgG-HRP (Cat#7074P2) and goat anti-mouse IgG-HRP were obtained from Cell Signaling Technology (Danvers, MA, USA) and Santa Cruz Biotechnology (Dallas, TX, USA), respectively.

Annexin V/PI Staining

To distinguish early and late apoptotic cell deaths, annexin V/PI staining was used. For this purpose, annexin V-FITC/PI apoptosis detection kit (Cat#HY-K1073, Med Chem Express, Monmouth Junction, NJ) was used as per the manufacturer's instructions. Briefly, HCT116 or BxPC-3 cells were seeded in 12-well plates. After specific time of treatment, cells were washed with cold 1X Dulbecco's phosphate-buffered saline phosphate buffered saline (DPBS) (Gibco, Grand Island, NY, USA), and trypsinized with 0.25 trypsin EDTA (Gibco, Grand Island, NY, USA). Trypsinized cells were resuspended with complete medium and centrifuged at 1,000g for 5 minutes at 4ºC. The media was discarded, and cells were resuspended with ice-cold PBS. Resuspended cells were again subjected to centrifugation and supernatant was discarded. Cells were resuspended in binding buffer followed by staining with annexin V-FITC and PI. The stained cells were incubated at room temperature for 10 minutes. After 10minutes, cells were then washed with PBS and treated with Hoechst for 10 minutes. To capture fluorescence images, an ECHO fluorescence microscope was used.

Mitochondria labeling

MitoTrackerTM Green FM kit (Cat#M7514, ThermoFischer Scientific, Carlsbad, CA, USA) was used to label mitochondria. HCT116 cells were incubated with MitoTracker Green FM dye after 24 h of ART, DZ-1 and DZ-1-ART treatment, according to manufacturer's instructions. Hoechst staining was done for visualizing the nucleus. To capture images, an ECHO fluorescence microscopy was used.

JC-1 Assay

To analyze mitochondrial membrane potential (ΔΨm), JC-1 dye (mitochondrial membrane potential probe, Cat#T3168, ThermoFisher Scientific, Eugene, OR, USA) was used. After 24 h of ART, DZ-1 and DZ-1-ART treatment, cells were stained with JC-1 dye as per the manufacturer's instructions and an ECHO fluorescence microscopy was used to capture images.

Lysosomes Labeling

To label lysosomes, LysoTracker™ Green DND-26 (Cat# L7526, ThermoFisher Scientific, ThermoFisher Scientific, Eugene, OR, USA) kit was used. After 24 treatment of ART, DZ-1, DZ-1-ART, cells were treated with LysoTracker probe containing media. To visualize nucleus, Hoechst staining was used. The images were captured using an ECHO fluorescence microscopy.

Statistical Analysis

One-way analysis of variance, followed by Tukey's post hoc test were used for statistical analysis. For this purpose, GraphPad Prism 9 software was used. Values are represented as mean ± standard deviation (SD) and P values of less than 0.05 were defined as statistically significant. Significance of P value is indicated as *P< 0.05, **P< 0.01, ***P< 0.001 ****P<0. 0001.

Results

DZ-1-ART induces apoptosis in time dependent manner.

DZ-1-ART was synthesized by conjunction of DZ-1 and ART (Fig. 1A). To define the time intervals effects of DZ-1-ART, HCT116 and BxPC-3 cells were treated with 20 µM of DZ-1- ART. After the treatments, both cells were harvested at 4 h, 8 h and 24 h and trypan blue exclusive assay was performed for cell survival analysis. The results from cell survival analysis clearly indicated the gradual increase of cellular cytotoxicity of DZ-1-ART in both HCT116 and BxPC-3 cells (Fig. 1B). Western blotting of DZ-1-ART treated cell lysates confirmed cleavage of poly (ADP-ribose) polymerase 1 (PARP-1), which implies the confirmation of apoptosis in HCT116 and BxPC-3 cells. Furthermore, cleaved caspase-8 and cleaved caspase-9 expression supported the involvement of DZ-1-ART-induced apoptosis (Fig. 1C). In addition, Annexin V- FITC/PI staining was performed for more confirmation. In both cells, early apoptosis was observed after 4 h of DZ-1-ART treatment while late apoptosis was observed in both 8 h and 24 h of the treatment (Fig. 1D&E).

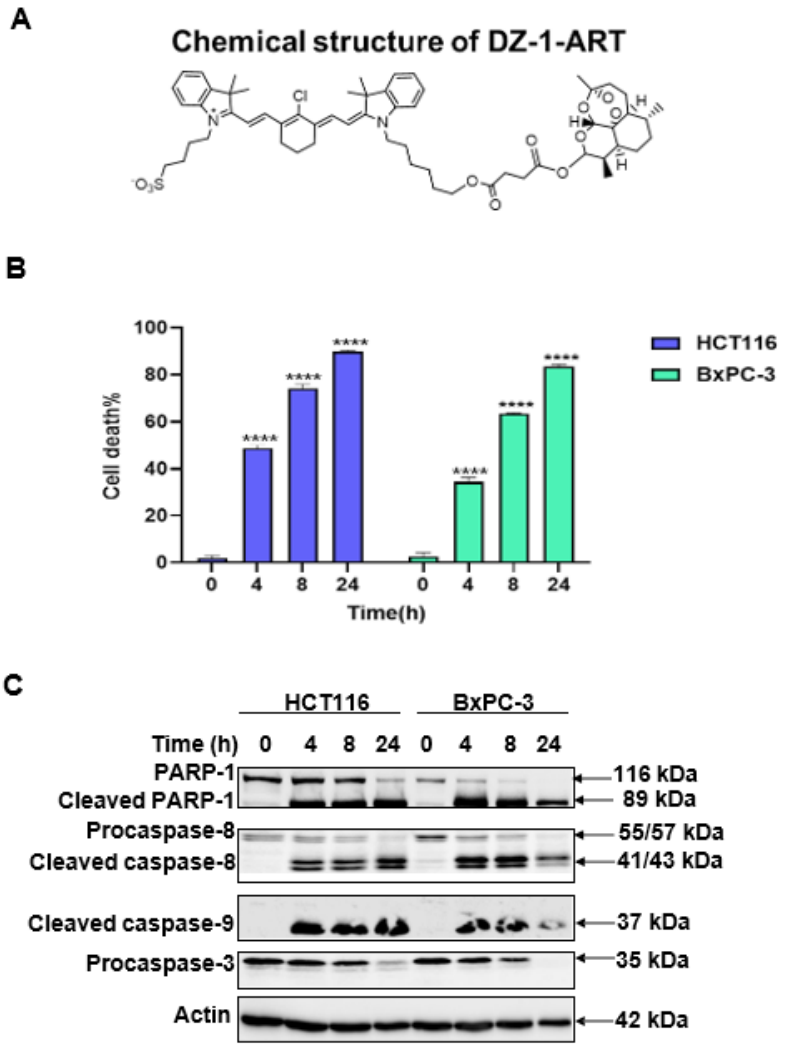

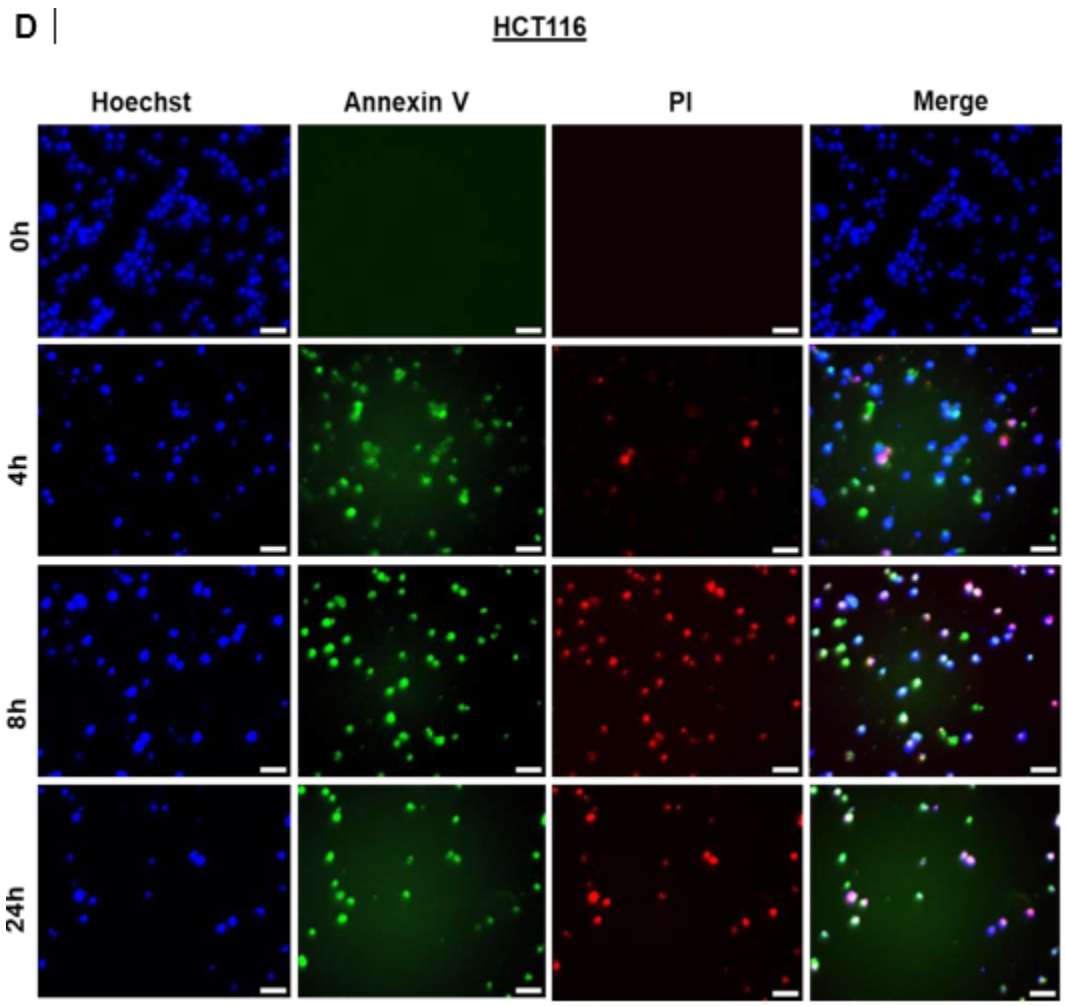
D
HCT116
Hoechst
Annexin V
PI
Merge
0h
4h
8h
24h

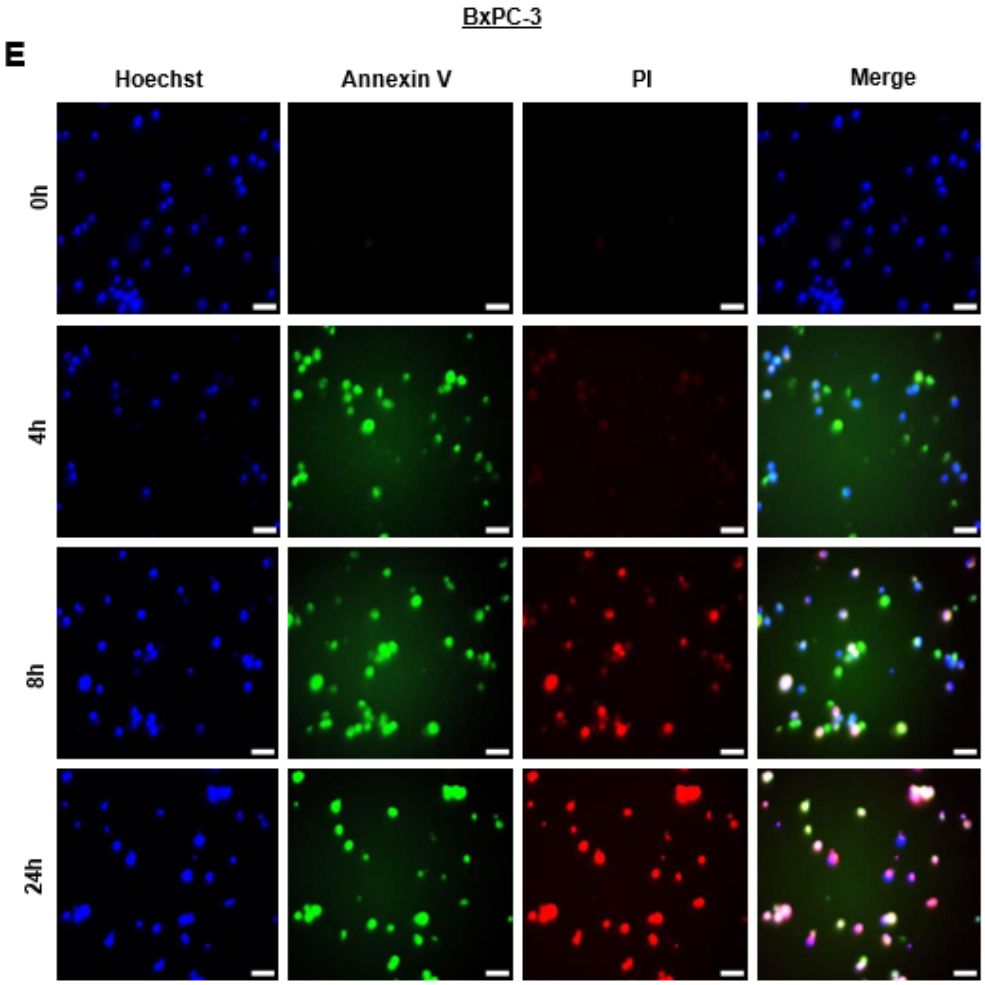

Figure 1: DZ-1-ART induces apoptosis in time dependent manner. (A) Chemical structure of DZ-1-ART. (B) HCT116 and BxPC-3 cells were treated with 20 µM of DZ-1-ART at various time intervals. Trypan blue exclusion assay was performed for cell survival analysis. For statistical analysis, one-way ANOVA and Tukey's multiple comparison test were used (****P<0.0001). From triplicate experiments, mean ± SD are shown as error bar. (C) Cells were harvested using 1X lysis buffer, followed by SDS-PAGE for immunoblotting analysis. Immunoblotting was performed using indicated antibodies. (D) and (E) Annexin V assay was performed for apoptosis detection in HCT116 and BxPC-3 cells.

DZ-1-ART localizes through lysosomes and mitochondria

Previous studies reported that DZ-1 conjugated analogs translocate via lysosomes and mitochondria [16,17]. Conjugation of ART with DZ-1 may alter its translocating pathways. To explore this, HCT-116 cells were treated with 10 µM of ART, DZ-1 and DZ-1-ART for 24 h.

After 24 h, treated cells were stained with LysoTracker Green DND-26 dye and Hoechst. DZ-1- ART treated cells showed higher (NIRF) red fluorescence than DZ-1 treated cells, while control and ART treated cells showed no red fluorescence. Green fluorescence (LysoTracker) was observed in control, ART, DZ-1 and DZ-1-ART treated cells, which confirmed lysosomes staining (Fig. 2A). Taken together, these results confirmed the lysosomal translocation of DZ-1- ART. To check the localization of DZ-1-ART via mitochondria, after 24 h of 10 µM treatment of ART, DZ-1 and DZ-1-ART, HCT116 cells were stained with MitoTracker Green FM dye. Fluorescence microscopy analysis indicated higher red (NIRF) fluorescence with green fluorescence (MitoTracker) in DZ-1-ART treated cells (Fig. 2B). These results supported the mitochondria mediated translocation of DZ-1-ART.

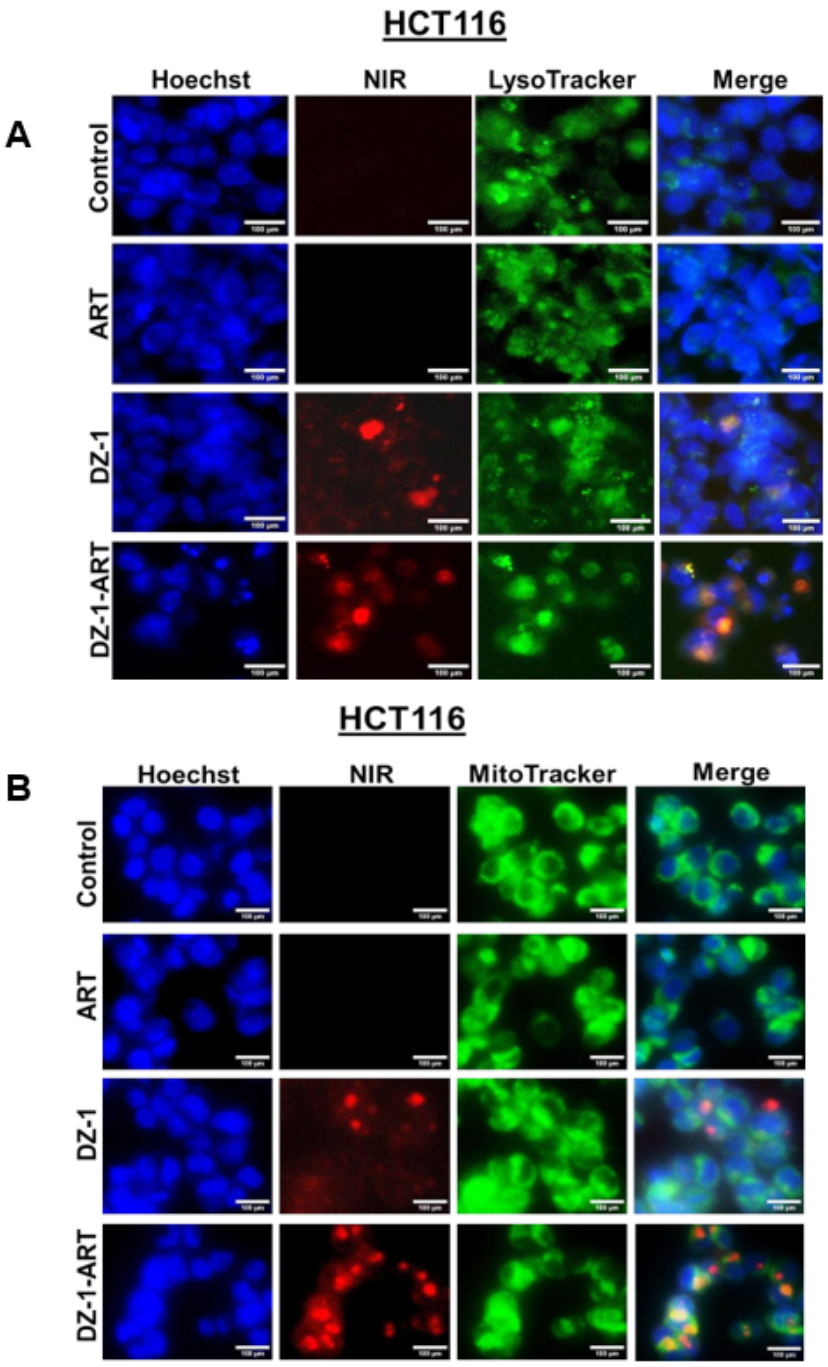

Figure 2: DZ-1-ART translocates through lysosomes and mitochondria. HCT116 cells were treated with 10 μM of ART, DZ-1 and DZ-1-ART for 24 h. (A) For lysosomal location, cells were stained with LysoTracker Green DND-26 dye. (B) Cells were stained with MitoTracker Green FM dye for mitochondrial localization assay. A fluorescence microscope was used to capture images (scale bar 100 μm).

Role of cathepsin B and cathepsin D in DZ-1-ART-induced apoptosis

The roles of cathepsin B (CatB) and cathepsin D (CatD) in DZ-1-ART-induced apoptosis were investigated, since LysoTracker staining revealed lysosomal localization of DZ-1-ART. To investigate CatB roles, HCT116 cells were treated with 10 µM of DZ-1-ART and CatB inhibitor, E-64 (25 µM and 50 µM). Trypan blue exclusion assay indicated high toxicity in 50 µM of E-64 alone and DZ-1-ART and 50 µM treated cells, which indicated cytotoxicity of 50 µM of E-64, whereas 25 µM of E-64 and DZ-1-ART treated cells showed no significant inhibition (Fig. 3A). Western blotting analysis also indicated no CatB mediated inhibition in DZ-1-ART-induced apoptosis (Fig. 3B). HCT116 cells were treated with 10 µM of DZ-1-ART and various concentrations of CatD inhibitor, pepstatin A (10 µM, 25 µM and 50 µM). Cell survival analysis indicated no significant difference between DZ-1-ART and DZ-1-ART with pepstatin A treated cells (Fig. 3C). Immunoblotting results confirmed no inhibition of PARP-1 cleavage in DZ-1- ART and pepstatin A treated cells when compared with DZ-1-ART treated cells (Fig. 4D).

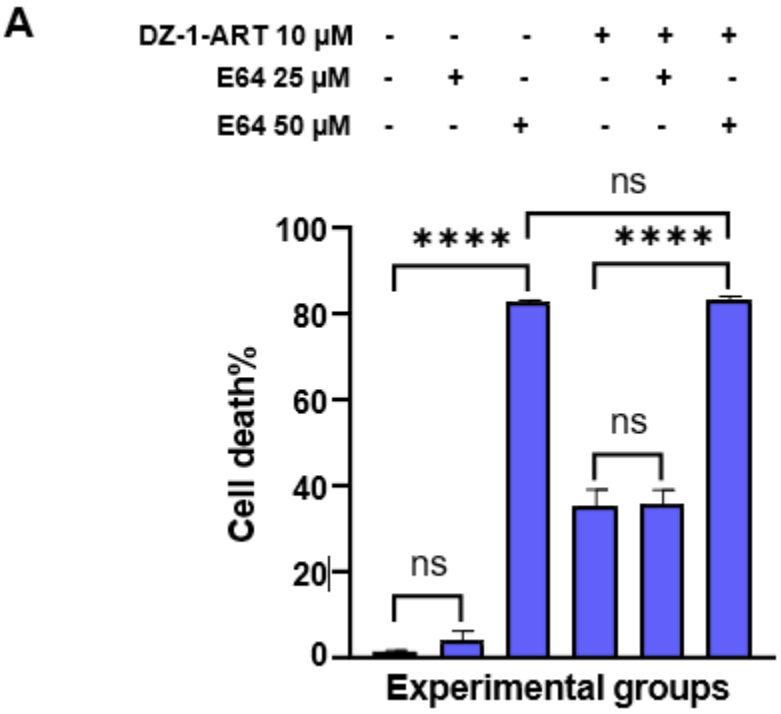

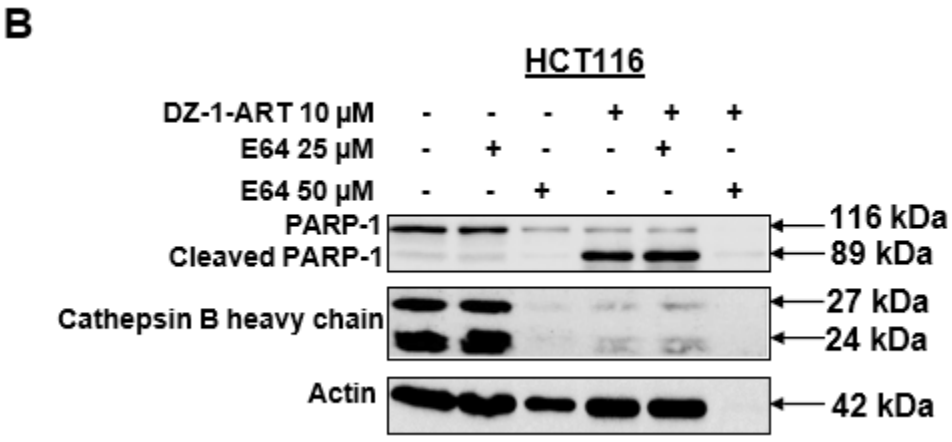

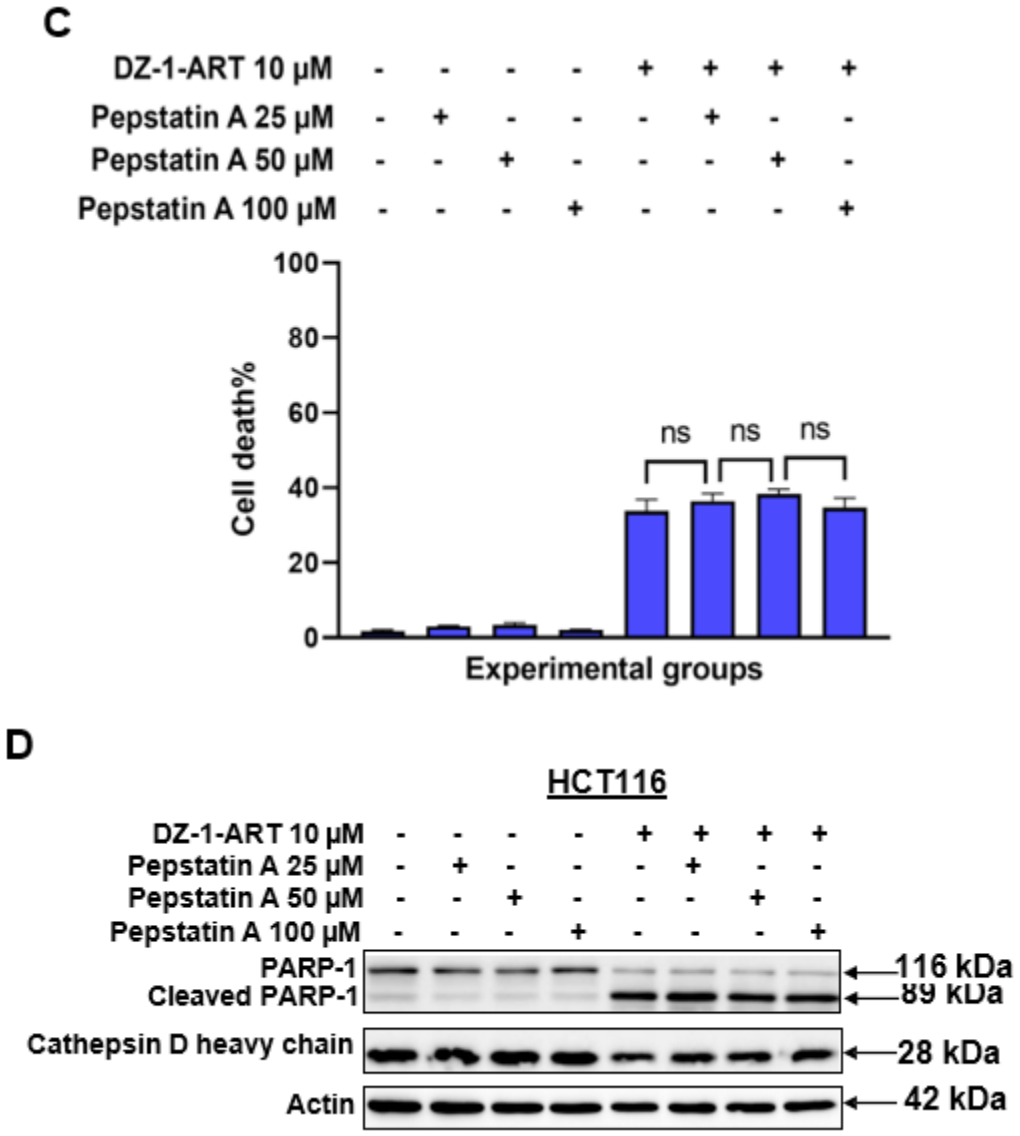

Figure 3: Role of cathepsin B and cathepsin D in DZ-1-ART-induced apoptosis. (A, B) HCT116 cells were treated with 25 µM and 50 µM of E-64 (cathepsin B inhibitor, with or without DZ-1-ART). (A) Trypan blue exclusion assay was performed for cell survival assay. (B) Treated cells were harvested using 1X lysis buffer then SDS -PAGE was performed for immunoblotting analysis. Membrane was developed using indicated antibodies. (C, D) For cathepsin D inhibition, HCT116 cells were treated with various concentration (25 µM, 50 µM and 100 µM) of pepstatin A (cathepsin D inhibitor, with or without DZ-1-ART). (C) Cell death per centage was quantified by trypan blue assay. (D) Immunoblotting was performed against indicated antibodies after cells harvesting and SDS-PAGE. For (A) and (C) values are shown as mean ± SD from triplicates. One-way ANOVA and Tukey's multiple comparison test were used for statistical analysis (****P <0.0001).

DZ-1-ART disrupts mitochondrial membrane potential

Since lysosomal-mediated cathepsins did not participate in DZ-1-ART-induced apoptosis, mitochondria-associated apoptosis was investigated. For this purpose, mitochondrial membrane potential (MMP) (Δψm) was measured in ART, DZ-1 and DZ-1-ART treated HCT116 cells. After 24 h of the treatments, cells were stained with JC-1 dye and followed by Hoechst staining. Fluorescence microscopy

analysis showed green fluorescence in DZ-1-ART treated cells, which indicated monomeric form of JC-1 dye. This green fluorescence confirmed the lower Δψm in DZ-1-ART treated cells. Red fluorescence ranges in control, ART and DZ-1 treated cells showed higher, medium and lower levels of intensity, respectively (Fig. 4). These results directly confirmed low Δψm in DZ-1-ART treated cells.

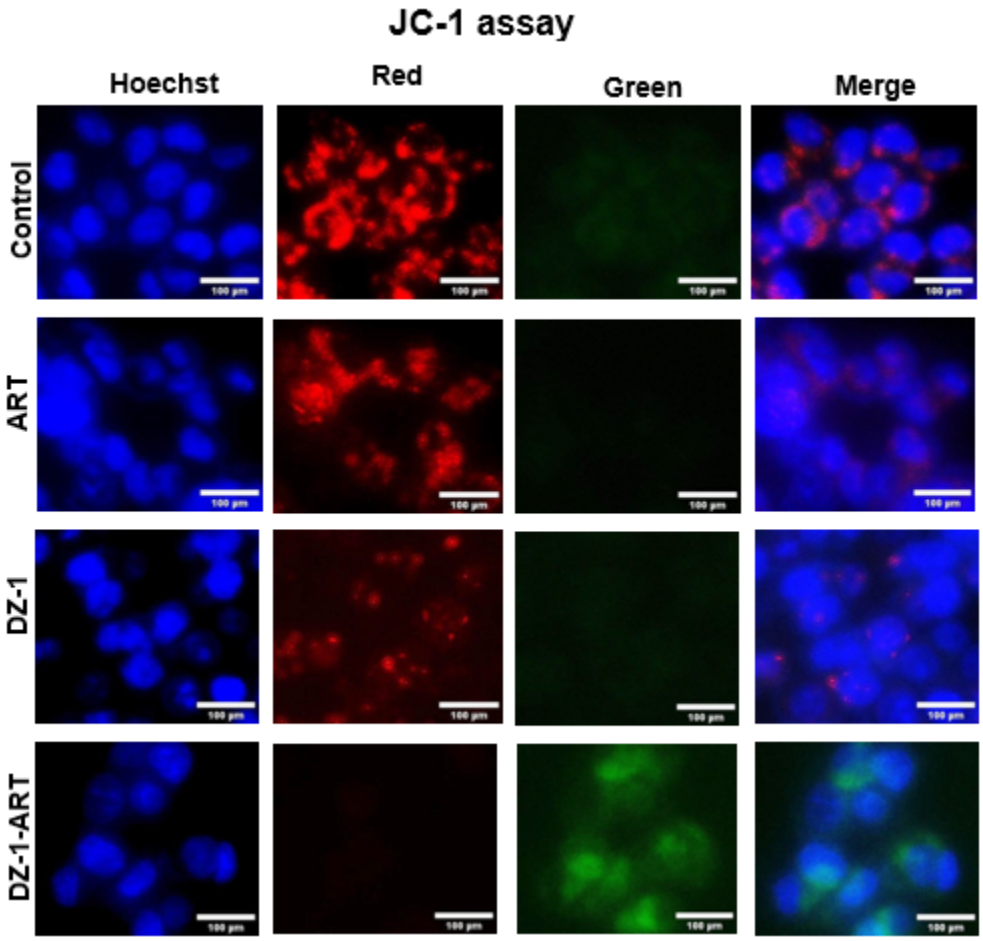

Figure 4: DZ-1-ART disrupts mitochondrial membrane potential. ART, DZ-1 and DZ-1-ART treated cells were stained with JC-1 dye and followed by Hoechst staining. Images were captured using a fluorescence microscope (scale bar:100 µm).

DZ-1-ART induces apoptosis through caspase activation pathways

Since JC-1 assay confirmed MMP disruption in HCT116 cells, caspase activation was investigated. For this purpose, HCT116 cells were treated with 10 µM of DZ-1-ART and various concentrations of pancaspase inhibitor, Z-VAD-FMK. Trypan blue exclusion assay results showed inhibition of cytotoxicity in DZ-1-ART and Z-VAD-FMK treated cells (dose-dependent manner) (Fig. 5A). Immunoblotting results showed inhibition of PARP-1 cleavage, cleaved caspase-8, cleaved caspase-9 and cleaved caspase-3 in DZ-1-ART and Z-VAD-FMK treated cells (Fig. 5B). Collectively, these results confirmed caspase activation pathways in DZ-1-ART treated cells. To define specific caspase involvement in DZ-1-ART-induced apoptosis, HCT116 cells were treated with 10 µM DZ-1-ART and various concentrations of caspase-3 inhibitor, Z- DEVD-FMK. Trypan blue assay revealed dose-dependent cytotoxicity inhibition in DZ-1-ART and Z-DEVD-FMK treated cells (Fig. 5C). Immunoblotting analysis reported inhibition of PARP-1 cleavage and caspase-3 cleavage in DZ-1-ART and Z-DEVD-FMK treated cells (Fig. 5D).

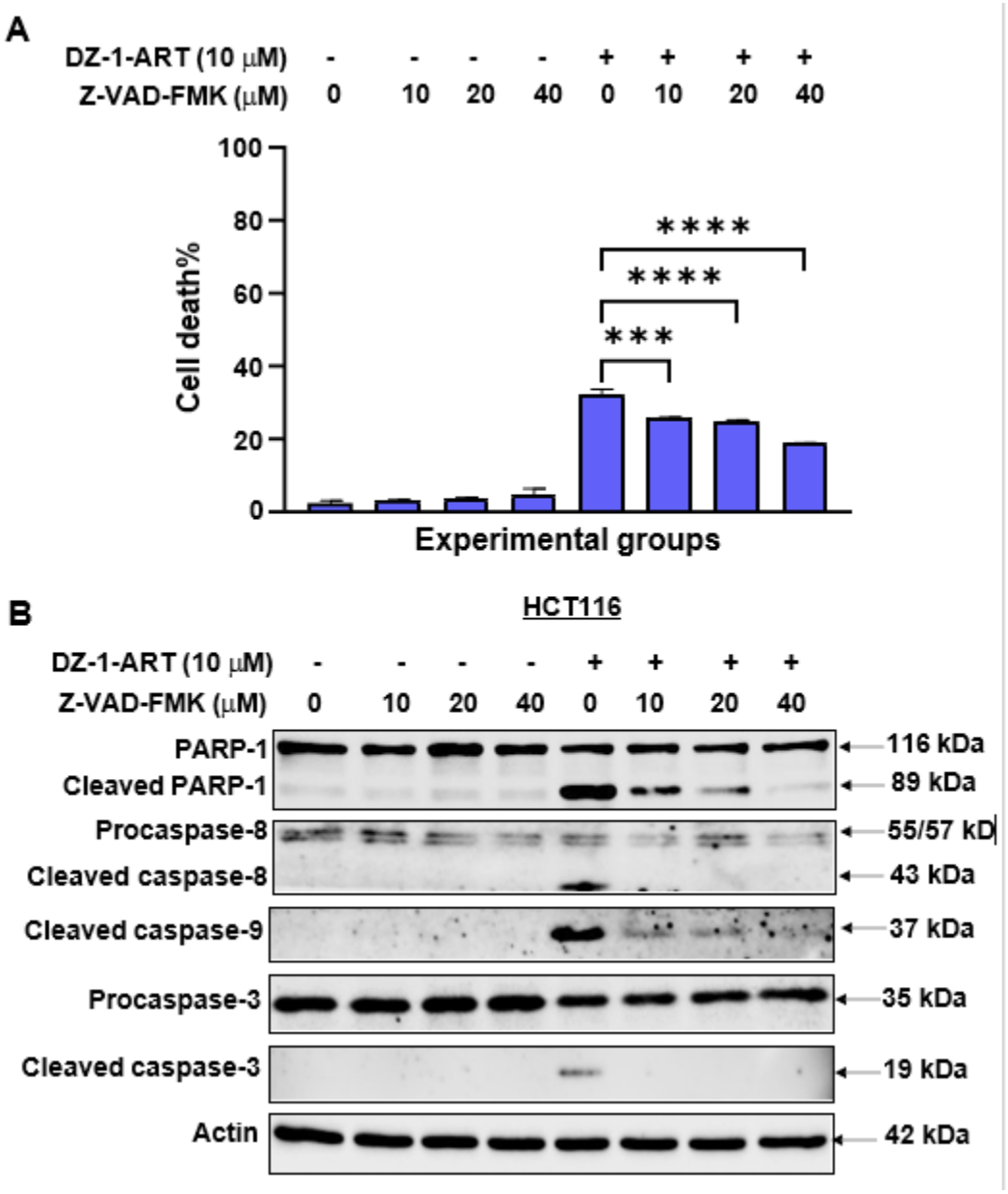
A
DZ-1-ART (10 μM) - - - - + + + +
Z-VAD-FMK (μM) 0 10 20 40 0 10 20 40
Cell death%
100
80
60
40
20
0
****
****
***
Experimental groups
B
HCT116
DZ-1-ART (10 μM) - - - - + + + +
Z-VAD-FMK (μM) 0 10 20 40 0 10 20 40
PARP-1
Cleaved PARP-1
Procaspase-8
Cleaved caspase-8
Cleaved caspase-9
Procaspase-3
Cleaved caspase-3
Actin
116 kDa
89 kDa
55/57 kD
43 kDa
37 kDa
35 kDa
19 kDa
42 kDa

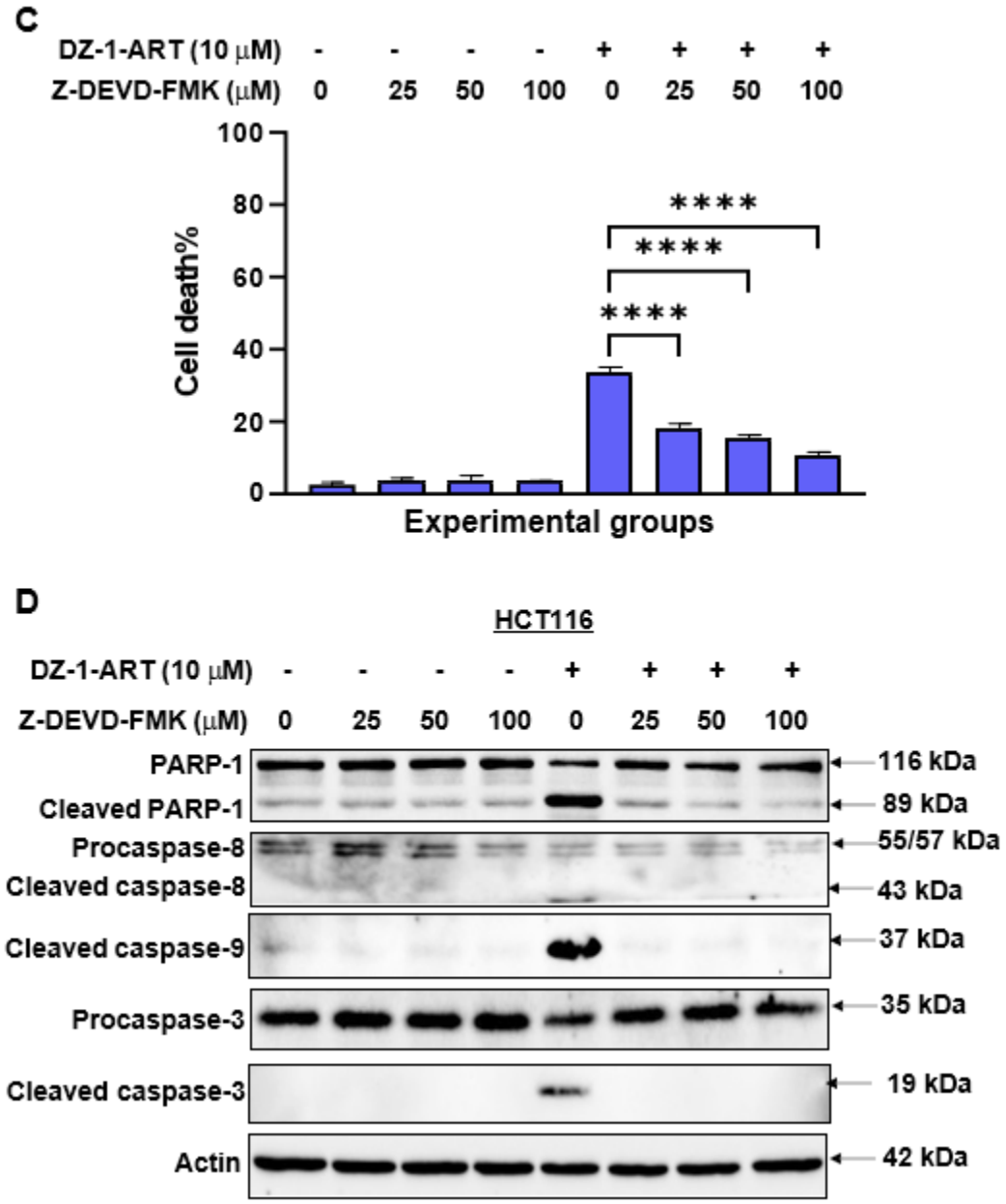

Figure 5: DZ-1-ART induces apoptosis through caspase activation pathways. (A, B) For pancaspase inhibition, HCT116 cells were pretreated with various concentrations of Z-VAD- FMK (10 μM, 20 μM and 40 μM), followed by 10 μM of DZ-1-ART. (A) Trypan blue exclusive assay was performed for cytotoxicity quantification. (B) Immunoblotting was used to detect indicated antibodies after harvesting treated cells. (C, D) For caspase-3 inhibition, various concentrations of Z-DEVD-FMK (25 μM, 50 μM and 100 μM) pretreated with HCT116 cells and followed by DZ-1-ART treatment. (C) For cytotoxicity quantification, trypan blue exclusive assay was performed. (D) HCT116 cells were harvested after 24 h of treatment, followed by SDS-PAGE. Immunoblotting was done for indicated antibodies. For (A) and (C), values represent mean ± SD from triplicates. For statistical analysis, one-way ANOVA and Tukey's multiple comparison test were used (****P <0.0001).

DZ-1-ART induces caspase-3-dependent apoptosis

MCF-7/Vector and MCF-7/Caspase 3 cells were treated with 20 µM of DZ-1-ART and harvested at various time points (4 h, 8 h and 12 h) for trypan blue exclusion assay. DZ-1-ART-induced cell death was observed after 4 h of treatment in MCF-7/Caspase 3 cells, while less cell death was seen in MCF-7/Vector cells (Fig. 6A). Immunoblotting results from DZ-1-ART treated MCF-7/Caspase 3 cells indicated time dependent manner of PARP-1 cleavage, whereas DZ-1- ART treated MCF-7/Vector cells showed no PARP-1 cleavage, due to absence of caspase 3 (Fig. 6B). Z-VAD-FMK and DZ-1-ART treatment at various time points (1-4 h) showed no effect in MCF-7/Vector cells (Fig. 6C), but the same treatment showed Z-VAD-FMK-mediated apoptosis inhibition in MCF-7/Caspase 3 cells (Fig. 6D). Taken together, these results confirmed caspase- 3-dependent apoptosis in DZ-1-ART-induced apoptosis.

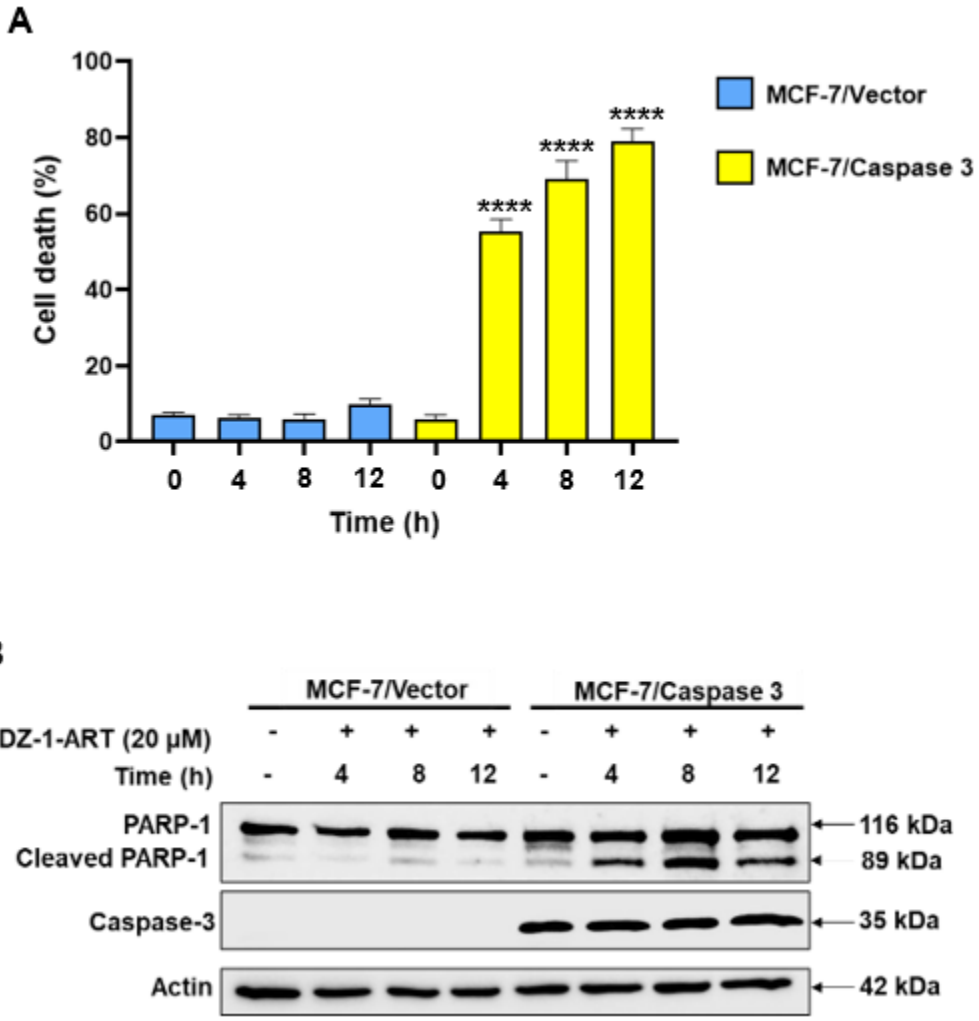

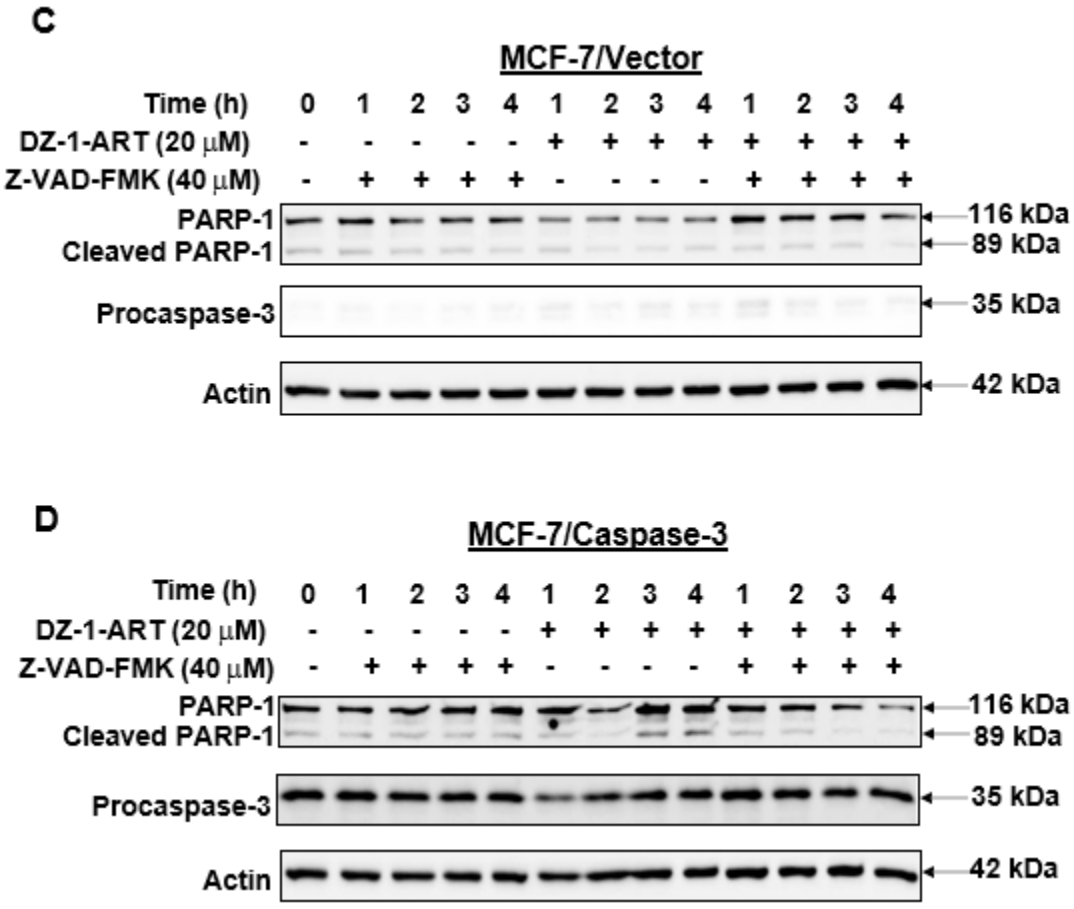

Figure 6: DZ-1-ART induces caspase-3-dependent apoptosis. (A, B) MCF-7/Vector and MCF- 7/Caspase 3 cells were treated with 20 μM of DZ-1-ART. (A) DZ-1-ART treated cells were trypsinized at various time intervals (4-12 h) for trypan blue exclusion assay. One-way ANOVA and Tukey's multiple comparison test were performed for statistical analysis, (****P <0.0001). (B) DZ-1-ART treated cells were harvested after indicated time intervals for immunoblotting. Harvested samples were subjected to SDS-PAGE and blotting to indicated antibodies. MCF-7/Vector cells (C) or MCF-7/Caspase 3 cells (D) were treated with 20 μM of DZ-1-ART and 40 μM of Z-VAD-FMK. These treated cells were harvested at various time intervals (1-4 h) and immunoblotting was performed using indicated antibodies.

DZ-1-ART induces Bax, Bak, and Bid-independent apoptosis

To confirm Bid involvement in DZ-1-ART-induced apoptosis, HCT116 WT and HCT116 Bid-/- cells were treated with 1 μM, 5 μM and 10 μM of DZ-1-ART. Cytotoxicity was observed in 10 μM DZ-1-ART treated HCT116 WT and HCT116 Bid-/- cells (Fig. 7A). Immunoblotting results indicated PARP-1 cleavage in both cells (Fig. 7B). These results supported Bid-independent apoptosis in DZ-1-ART-induced apoptosis. To reveal Bax and Bak roles in DZ-1-ART-induced apoptosis, HCT116 WT, HCT116 Bax-/-, HCT116 Bak-/-, HCT116 Bax-/-Bak-/- cells were treated with 5 μM and 10 μM of DZ-1-ART. Significant cell deaths were observed in 10 μM DZ-1- ART treated HCT116 WT, HCT116 Bax-/-, HCT116 Bak-/- and HCT116 Bax-/-Bak-/- cells (Fig. 7C).Western blotting analysis indicated PARP-1 cleavage in 10 μM DZ-1-ART treated cells (Fig. 7D). These results confirmed Bax and Bak-independent apoptosis of DZ-1-ART-induced apoptosis.

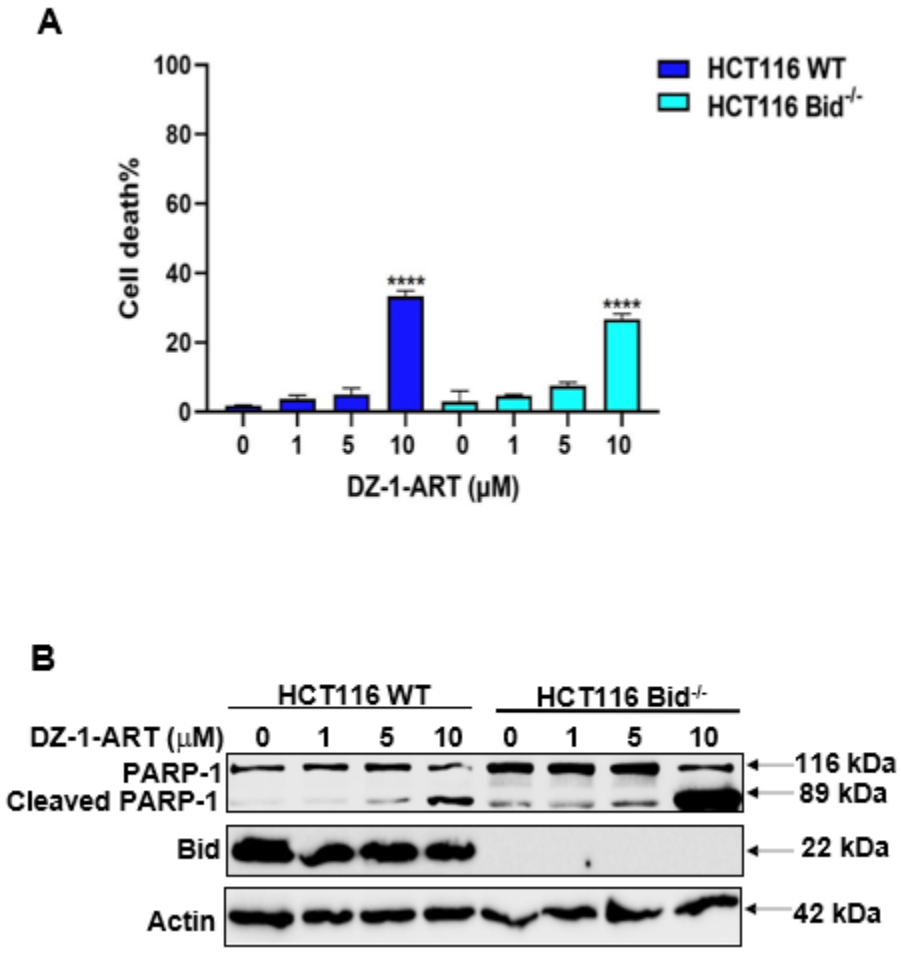
A
HCT116 WT
HCT116 Bid-/-
Cell death%
100
80
60
40
20
0
****
****
0 1 5 10 0 1 5 10
DZ-1-ART (μM)
B
HCT116 WT
HCT116 Bid-/-
DZ-1-ART (μM) 0 1 5 10 0 1 5 10
PARP-1
Cleaved PARP-1
116 kDa
89 kDa
Bid
22 kDa
Actin
42 kDa

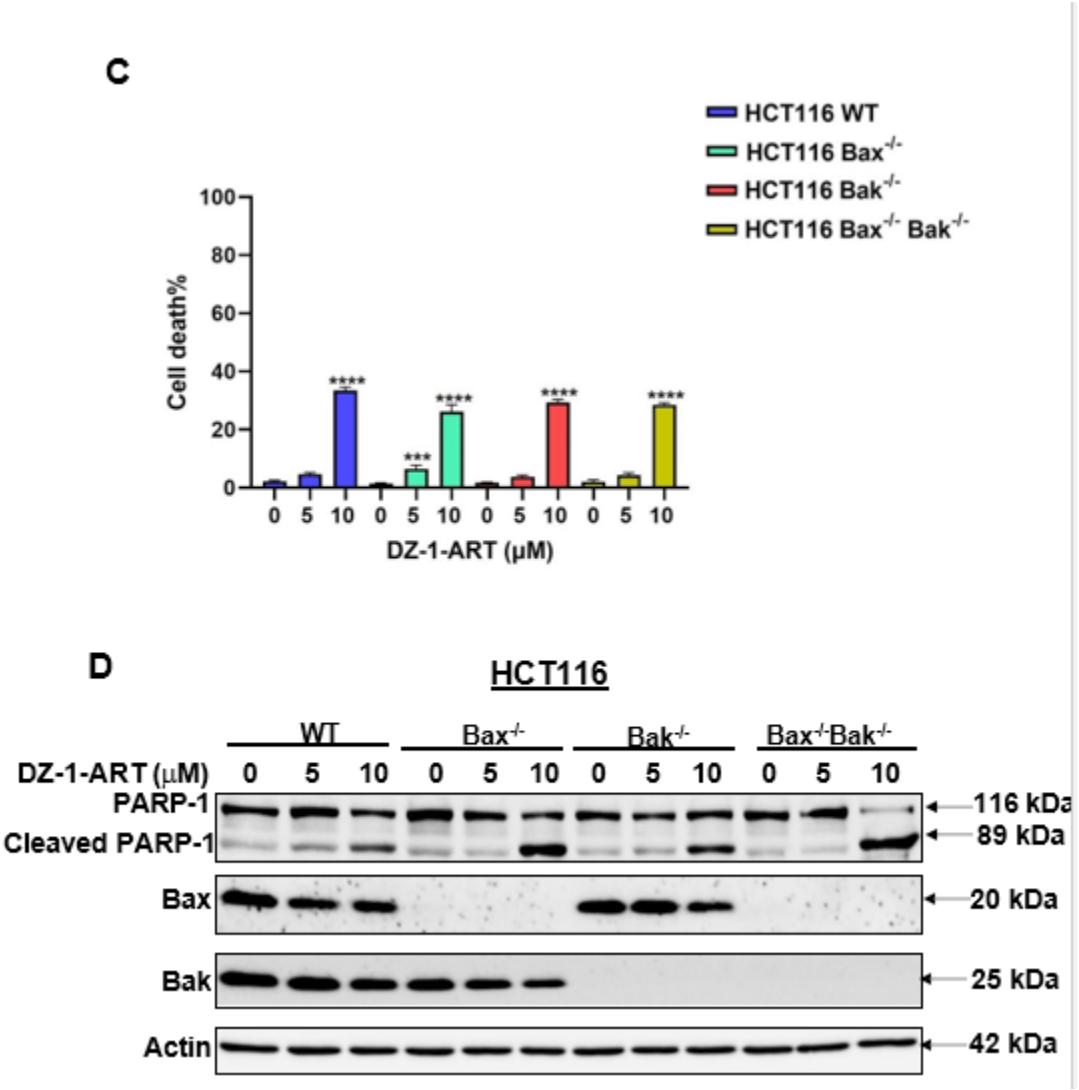

Figure 7: DZ-1-ART induces Bax, Bak, and Bid-independent apoptosis. (A, B) HCT116 WT, HCT116 Bid-/- cells were treated with 1 μM, 5 μM and 10 μM of DZ-1-ART. (A) After 24 h of treatment, cells were trypsinized for cell survival analysis. (B) Immunoblotting was performed for indicated antibodies. (C, D) HCT116 WT, HCT116 Bax-/-, HCT116 Bak-/- and HCT116 Bax-/- Bak-/- cells were subjected to 5 μM and 10 μM of DZ-1-ART treatment for 24 h. (C) The treated cells were trypsinized for trypan blue exclusion assay. (D) The treated cells were harvested and immunoblotting was performed for indicated antibodies. For (A) and (C), one-way ANOVA and Tukey's multiple comparison test were done for statistical analysis, (****P<0.0001).

Discussion

Targeting therapy enables specific targeting and killing of tumor cells while unaffecting normal cells. To achieve these properties, anticancer agents can be conjugated with biopolymers, small molecules and fluorescence dyes. In this study, DZ-1-ART (conjugated form of ART with NIR dye DZ-1) has been used and cytotoxicity and cell death mechanisms have been evaluated in vitro. This study reveals time-dependent manner DZ-1-ART-induced cytotoxicity in HCT116 and BxPC-3 cells (Fig. 1A), and MCF-7 cells (Fig. 5). It also shows apoptosis-mediated cell death through caspases activation (Fig. 1B). ART induces ferroptosis in various cancer cells [28-31]. However, conjugation of ART and DZ-1 may alter the mechanism of cell death.

DZ-1-ART accumulates through lysosomes and mitochondria (Fig. 2A&B), like DZ-1 conjugated analog, DZ-cisplatin (DZ-CIS) [24]. The long aliphatic and cationic structure of DZ- 1-ART perhaps leads to its accumulation in lysosomes and mitochondria. CatB and CatD release from lysosomes play vital roles in apoptosis [32, 33]. But this study shows no CatB and CatD roles in DZ-1-ART-induced apoptosis.

Mitochondrial localization of DZ-1-ART can cause MMP disruption. JC-1 assay results showed MMP disruption in DZ-1-ART treated cells (Fig. 4). MMP disruption can induce caspases activation, while Z-VAD-FMK and Z-DEVD-FMK treatment with DZ-1-ART inhibits caspase activation (Fig. 5A, B, C&D). Furthermore, this study has confirmed an involvement of caspase-3 in DZ-1-ART-induced apoptosis in MCF-7/Caspase 3 cells, while MCF-7/Vector has shown no apoptosis due to caspase-3 absence (Fig. 6B).

Proapoptotic proteins such as Bid, Bax and Bak are involved in mitochondrial outer membrane pore formation for cytochrome C release [34]. This study shows apoptosis-mediated cytotoxicity in DZ-1-ART treated HCT116 Bid-/-, HCT116 Bax-/-, HCT116 Bak-/- and HCT116 Bax-/- Bak-/- cells (Fig. 7A, B, C&D). These results have shown that DZ-1-ART can induce Bid, Bax and Bak-independent apoptosis. Previously, few studies have shown Bid, Bax/Bak- independent apoptosis mediated through ER stress and serine proteases-dependent mechanism [35, 36]. DZ-1-ART-induced, Bid, Bax/Bak-independent apoptosis could be associated with ER stress related signals that may not be reliant on Bax and Bak pore formation.

Another possible mechanism of DZ-1-ART-induced Bax/Bak-independent apoptosis is mitochondrial lipid peroxidation which leads to mitochondrial membrane damage. The mitochondrial localization of DZ-1-ART may induces ROS generation in mitochondria. Since ester is used to conjugate DZ-1 to ART, DZ-1-ART perhaps cleaved into DZ-1 and ART by esterase in the mitochondria. An endoperoxide bridge of cleaved ART may induce ROS generation such as superoxide and hydroxy radicals through iron mediated fenton-like reactions. Since Fe^{2+} concentration in the mitochondria of tumor cells (20-30 μM) is higher than that in the cytosol (0.5-2 μM) [37, 38], ART effectively generates ROS in the mitochondria. These generated ROS may oxidize and damage lipids in the mitochondrial membranes through lipid peroxidation. Damage in the mitochondrial membrane can lead to mitochondrial depolarization, lower $\Delta\psi m$ and dysfunction. These events may induce opening of mitochondrial permeability pores thereby promoting the release of cytochrome C and activating caspase signaling pathway. Obviously, further studies are necessary to understand the molecular mechanism of DZ-1-ART- induced ROS-mediated apoptosis.

Since DZ-1-ART preferentially targets and kills cancer cells while not affecting normal cells, we may be able to develop a combined therapy. We previously reported that ART in combination with tumor necrosis factor-related apoptosis-inducing ligand (TRAIL) can enhance apoptosis in cancer cells [39]. ART-induced ER stress signals are integrated with TRAIL- induced apoptosis signals and promote apoptosis [40]. Nevertheless, these anticancer efficacies of ART can be limited due to nonspecific targeting and toxicity. To overcome these limitations, DZ-1-ART can be used for precise targeting and killing of cancer cells. The results from this study have supported that the combined treatment with DZ-1-ART and TRAIL can be developed as a theranostic agent to localize tumor and kill cancer cells. Obviously, these possibilities need to be further studied to reveal tumoricidal efficacy of the combined treatment in tumors.

Rhein-ART conjugate-induced ER stress and immunogenic cell death (ICD) have been reported in 4T1 cancer model [41]. Similarly, DZ-1-ART-induced ROS could trigger ER stress in cancer cells. As a result, ER stress can induce the translocation of calreticulin (CRT) from the ER lumen to the membrane surface. The membrane surface- exposed CRT could act as an “eat- me” signal to dendritic cells (DCs) and macrophages. Phagocytosis of cancer cells by DCs and macrophages, possibly process tumor antigens for T-cell activation. These proposed mechanisms of immunomodulatory effect of DZ-1-ART could be considered for immunotherapeutic purposes. Therefore, future studies are warranted to investigate these mechanisms.

In summary, this study reveals that lysosomes and mitochondria mediate cellular uptake of DZ-1-ART, DZ-1-ART-induced cell death through mitochondria associated apoptosis via activation of caspase signaling pathways. Interestingly, DZ-1-ART executes apoptosis via Bid, Bax/Bak-independent, but caspase-3-dependent manners.

Acknowledgments

This work was supported by the following grants: National Institutes of Health R21CA259243 (Y.J.L), R01CA265827 (Y.J.L.), R21CA256419 (Y.Z), and Department of Defense W81XWH- 22-1-1095 RA210084 (Y.J.L.).

Declaration of Interest Statement: DZ-1-ART is licensed to DaZen Theranostics, Inc., of which Yi Zhang is a shareholder position. A joint patent for DZ-1-ART (US20230226198A1) has been filed. Other authors declare no competing financial interests.

Declarations

Ethical Approval: Not applicable

Availability of data and materials: Research materials that were generated in the studies will be made freely available to

the scientific research community as soon as this manuscript has been documented in a publication. Raw data were generated at the Cedars-Sinai Medical Center. Derived data supporting the findings of this study are available from the corresponding author Dr. Yong J. Lee on request.

Author Contributions

B.N. and S.H. were responsible for the data collection and analysis. Y.Z. produced DZ-1-ART. A.G. provided tumor tissues. Y.J.L. H.L., C.S., H-N. W., and B.N. were responsible for the study conception and design. Y.J.L. and B.N. were responsible for writing the manuscript.

References

1. Khanal P (2021) Antimalarial and anticancer properties of artesunate and other artemisinins: current development. Monatsh Chem 152:387–400.
2. Krishna S, Bustamante L, Haynes RK, Staines HM (2008) Artemisinins: their growing importance in medicine. Trends Pharmacol Sci 29:520–27.
3. Zheng D, Liu T, Yu S, Liu Z, Wang J, et al. (2024) Antimalarial Mechanisms and Resistance Status of Artemisinin and Its Derivatives. Trop Med Infect Dis 9:223.
4. Berköz M, Özkan-Yılmaz F, Özlüer-Hunt A, Krośniak M, Türkmen Ö, et al. (2021) Artesunate inhibits melanoma progression in vitro via suppressing STAT3 signaling pathway. Pharmacol Rep 73:650–63.
5. Michaelis M, Kleinschmidt MC, Barth S, Rothweiler F, Geiler J, Breitling R, et al. (2010) Anti-cancer effects of artesunate in a panel of chemoresistant neuroblastoma cell lines. Biochem Pharmacol 79:130–6.
6. Yao X, Zhao C ru, Yin H, Wang K, Gao J Jun (2020) Synergistic antitumor activity of sorafenib and artesunate in hepatocellular carcinoma cells. Acta Pharmacol Sin 41:1609–20.
7. Niederreiter M, Klein J, Arndt K, Werner J, Mayer B (2023) Anti-Cancer Effects of Artesunate in Human 3D Tumor Models of Different Complexity. Int J Mol Sci 24:7844.
8. Fan X, Yan Y, Li Y, Song Y, Li B (2025) Anti-tumor mechanism of artesunate. Front Pharmacol 15:1483049.
9. Huang Z, Gan S, Zhuang X, Chen Y, Lu L, et al. (2022) Artesunate Inhibits the Cell Growth in Colorectal Cancer by Promoting ROS-Dependent Cell Senescence and Autophagy. Cell 11:2472.
10. Chen Y, Wang F, Wu P, Gong S, Gao J, et al. (2021) Artesunate induces apoptosis, autophagy and ferroptosis in diffuse large B cell lymphoma cells by impairing STAT3 signaling. Cell Signal 88:110167.
11. Kim C, Lee JH, Kim SH, Sethi G, Ahn KS (2015) Artesunate suppresses tumor growth and induces apoptosis through the modulation of multiple oncogenic cascades in a chronic myeloid leukemia xenograft mouse model. Oncotarget 6:4020–35.
12. Du JH, Zhang HD, Ma ZJ, Ji KM (2010) Artesunate induces oncosis-like cell death in vitro and has antitumor activity against pancreatic cancer xenografts in vivo. Cancer Chemother Pharmacol 65:895–902.
13. Deeken JF, Wang H, Hartley M, Cheema AK, Smaglo B, et al. (2018) A phase I study of intravenous artesunate in patients with advanced solid tumor malignancies. Cancer Chemother Pharmacol 81:587–96.
14. Nguyen HT, Tran TH, Kim JO, Yong CS, Nguyen CN (2015) Enhancing the in vitro anti-cancer efficacy of artesunate by loading into poly-d, l-lactide-co-glycolide (PLGA) nanoparticles. Arch Pharm Res 38:716–24.
15. Ho HN, Do TT, Nguyen TC, Yong CS, Nguyen CN (2020) Preparation, characterisation and in vitro/in vivo anticancer activity of lyophilised artesunate-loaded nanoparticles. J Drug Deliv Sci Technol 58:10180.
16. Yang X, Shi C, Tong R, Qian W, Zhau HE et al. (2010) Near IR Heptamethine Cyanine Dye– Mediated Cancer Imaging. Clin Cancer Res 10:2833–44.
17. Yang H, Liu Z, Li X, Zhang Z, Chen D, et al. (2018) Artesunate-Loaded and Near-Infrared Dye- Conjugated Albumin Nanoparticles as High-Efficiency Tumor-Targeted Photo-Chemo Theranostic Agent. Nanoscale Res Lett 13:319.
18. Choi PJ, Park TI, Cooper E, Dragunow M, Denny WA, et al. (2020) Heptamethine Cyanine Dye Mediated Drug Delivery: Hype or Hope. Bioconjugate Chem 31:1724–39.
19. Zhang C, Liu T, Su Y, Luo S, Zhu Y, et al. (2010) A near-infrared fluorescent heptamethine indocyanine dye with preferential tumor accumulation for in vivo imaging. Biomaterials 31:6612–7.
20. Zhang C, Zhao Y, Zhang H, Chen X, Zhao N, et al. (2017) The Application of Heptamethine Cyanine Dye DZ-1 and Indocyanine Green for Imaging and Targeting in Xenograft Models of Hepatocellular Carcinoma. Int J Mol Sci 6:1332.
21. Shi C, Wu JB, Chu GCY, Li Q, Wang R, et al. (2004) Heptamethine carbocyanine dye- mediated near-infrared imaging of canine and human cancers through the HIF-1α/OATPs signaling axis. Oncotarget 5:10114–26.
22. Wu JB, Shao C, Li X, Shi C, Li Q, et al. (2014) Near-infrared fluorescence imaging of cancer mediated by tumor hypoxia and HIF1α/OATPs signaling axis. Biomaterials 35:8175–85.
23. Ou Y, Wang R, Chu GC, Elmadbouh OHM, Lim A, et al. (2022) Novel DZ□SIM Conjugate Targets Cancer Mitochondria and Prolongs Survival in Pancreatic Ductal Adenocarcinoma. Adv Ther 5:2200021.
24. Mrdenovic S, Zhang Y, Wang R, Yin L, Chu GC, et al. (2019) Targeting Burkitt lymphoma with a tumor cell–specific heptamethine carbocyanine□cisplatin conjugate. Cancer 125:2222–32.
25. Mrdenovic S, Wang Y, Yin L, Chu GCY, Ou Y, et al. (2023) A cisplatin conjugate with tumor cell specificity exhibits antitumor effects in renal cancer models. BMC Cancer 23:499.
26. Ou Y, Chu GCY, Lyu J, Yin L, Lim A, et al. (2024) Overcoming Resistance in Prostate Cancer Therapy Using a DZ-Simvastatin Conjugate. Mol Pharmaceutics 21:873–82.
27. Nam SY, Amoscato AA, Lee YJ (2002) Low glucose-enhanced TRAIL cytotoxicity is mediated through the ceramide–Akt–FLIP pathway. Oncogene 21:337–46.
28. Roh JL, Kim EH, Jang H, Shin D (2017) Nrf2 inhibition reverses the resistance of cisplatin-resistant head and neck cancer cells to artesunate-induced ferroptosis. Redox Biol 11:254–62.
29. Wang K, Zhang Z, Wang M, Cao X, Qi J, et al. (2019) Role of GRP78 inhibiting artesunate- induced ferroptosis in KRAS mutant pancreatic cancer cells. Drug Des Devel Ther 13:2135–44.
30. Song Q, Peng S, Che F, Zhu X (2022) Artesunate induces ferroptosis via modulation of p38 and ERK signaling pathway in glioblastoma cells. J Pharmacol Sci 148:300–6.
31. Huang R, Xu R, Shi J, Yang Z, Zheng J, et al. (2015) Artesunate

induces ferroptosis in osteosarcoma through NCOA4-mediated ferritinophagy. FASEB J 39:e70488.

32. Xie Z, Zhao M, Yan C, Kong W, Lan F, et al. (2023) Cathepsin B in programmed cell death machinery: mechanisms of execution and regulatory pathways. Cell Death Dis 14:255.
33. Marques C, Oliveira CSF, Alves S, Chaves SR, Coutinho OP, et al. (2013) Acetate- induced apoptosis in colorectal carcinoma cells involves lysosomal membrane permeabilization and cathepsin D release. Cell Death Dis 4:e507.
34. Korsmeyer SJ, Wei MC, Saito M, Weiler S, Oh KJ, et al. (2000) Pro-apoptotic cascade activates BID, which oligomerizes BAK or BAX into pores that result in the release of cytochrome c. Cell Death Differ 7:1166–73.
35. Mizuta T, Shimizu S, Matsuoka Y, Nakagawa T, Tsujimoto Y (2007) A Bax/Bak-independent Mechanism of Cytochrome c Release. J Biol Chem 282:16623–30.
36. Zamorano S, Rojas-Rivera D, Lisbona F, Parra V, Court FA, et al. (2012) A BAX/BAK and Cyclophilin D-Independent Intrinsic Apoptosis Pathway. PLoS One 7:e37782.
37. Ni S, Kuang Y, Yuan Y, Yu B (2020) Mitochondrion-mediated iron accumulation promotes carcinogenesis and Warburg effect through reactive oxygen species in osteosarcoma. Cancer Cell Int 20:399.
38. Tam E, Sung HK, Lam NH, You S, Cho S, et al. (2023) Role of Mitochondrial Iron Overload in Mediating Cell Death in H9c2 Cells. Cells 12:118.
39. Lee YS, Lee DH, Jeong SY, Park SH, Oh SC, et al. (2019) Ferroptosis-inducing agents enhance TRAIL-induced apoptosis through upregulation of death receptor 5. J Cell Biochem 120:928–39.
40. Hong SH, Lee DH, Lee YS, Jo MJ, Jeong YA, et al. (2017) Molecular crosstalk between ferroptosis and apoptosis: emerging role of ER stress-induced p53-independent PUMA expression. Oncotarget 8:115164–78.
41. Xu ZJ, Wang W, Huang SW (2024) The Conjugate of Rhein–Artesunate for Inducing Immunogenic Cell Death to Prepare Cancer Vaccine and Suppress Tumor Growth. Chemistry 6:345–60.